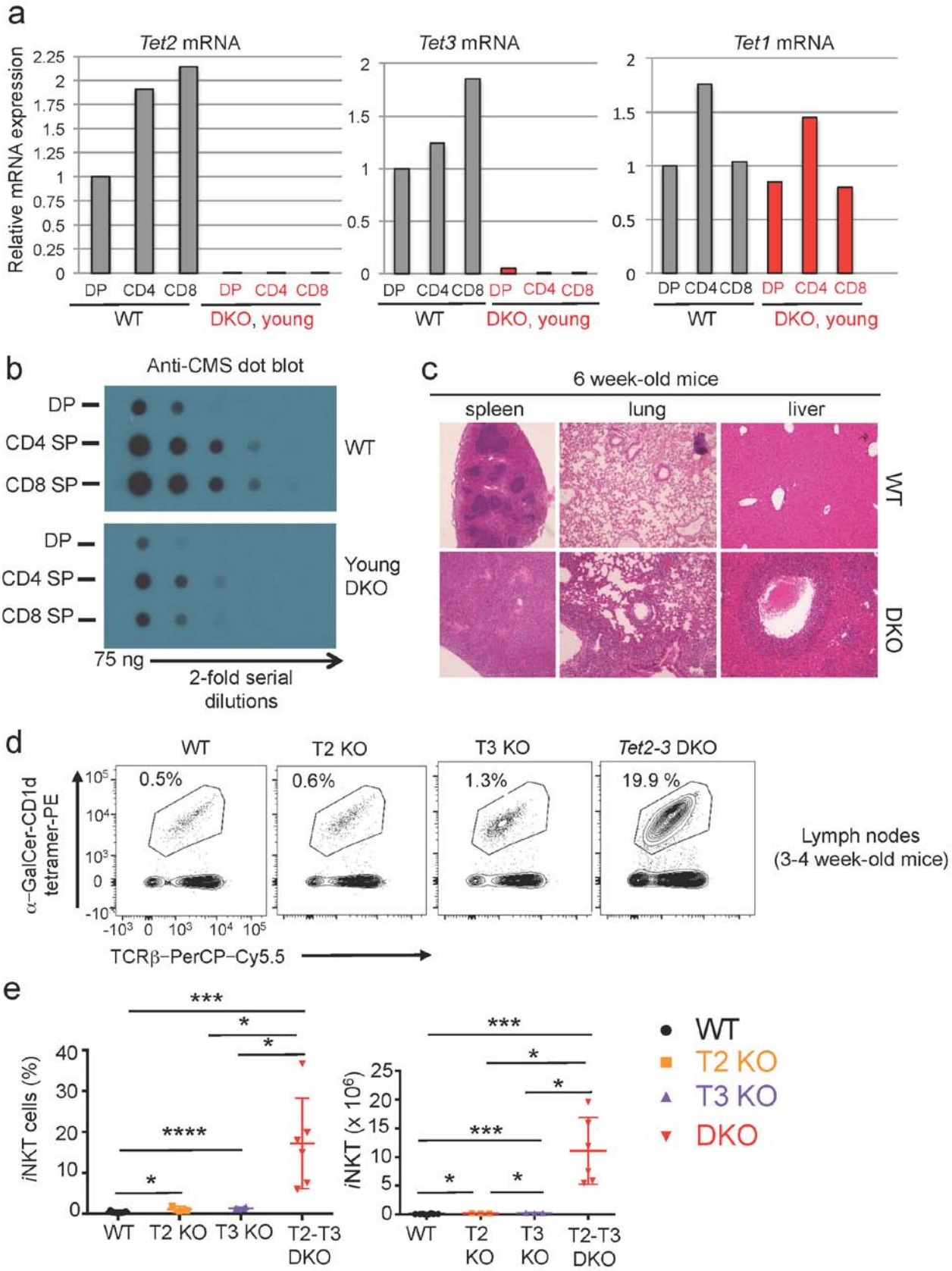
a
Tet2 mRNA
Tet3 mRNA
Tet1 mRNA
Relative mRNA expression
DP CD4 CD8 DP CD4 CD8
WT
DKO, young
b
Anti-CMS dot blot
DP
CD4 SP
CD8 SP
WT
Young DKO
75 ng
2-fold serial dilutions
c
6 week-old mice
spleen
lung
liver
WT
DKO
d
WT
T2 KO
T3 KO
Tet2-3 DKO
0.5%
0.6%
1.3%
19.9 %
α-GalCer-CD1d tetramer-PE
TCRβ-PerCP-Cy5.5
Lymph nodes (3-4 week-old mice)
e
iNKT cells (%)
iNKT (× 10^6)
WT
T2 KO
T3 KO
T2-T3 DKO

Supplementary Figure 1

Characterization of *Tet2-3* DKO mice

(a) *Tet1*, *Tet2* and *Tet3* mRNA expression assessed by quantitative RT-PCR. PolyA+ RNA was isolated from DP, CD4 SP and CD8 SP T cells from wild type (WT) and *Tet2*$^{-/-}$*Tet3*$^{fl/fl}$ CD4cre (*Tet2-3* DKO) mice. Relative mRNA expression levels were normalized to *Gapdh*.

(b) 5hmC levels in genomic DNA of thymocyte subsets from WT (n=2) and *Tet2-3* DKO (n=2) mice, estimated by anti-CMS dot blot after bisulfite treatment of genomic DNA to convert 5hmC to CMS. One representative experiment out of 2 is shown.

(c) Haematoxylin and eosin staining of spleen, lung and liver sections from 6 week-old control (upper panel) and *Tet2-3* DKO (lower panel) mice.

(d) *i*NKT cells in lymph nodes (LN) of WT versus *Tet2*$^{-/-}$, *Tet3 KO* and *Tet2-3* DKO *i*NKT cells as defined by $\tilde{\alpha}$GalCer-CD1d and TCRβ staining.

(e) Percentage (*left*) and number (*right*) of *i*NKT cells in lymph nodes. n=6 (WT), n=3 (*Tet2* KO), n=at least 2 (*Tet3* KO), n=6 (*Tet2/3 DKO*).

Data are mean $\pm$ SEM. *P<0.05, **P< 0.01, ***P< 0.001, ****P< 0.0001 (unpaired t test)

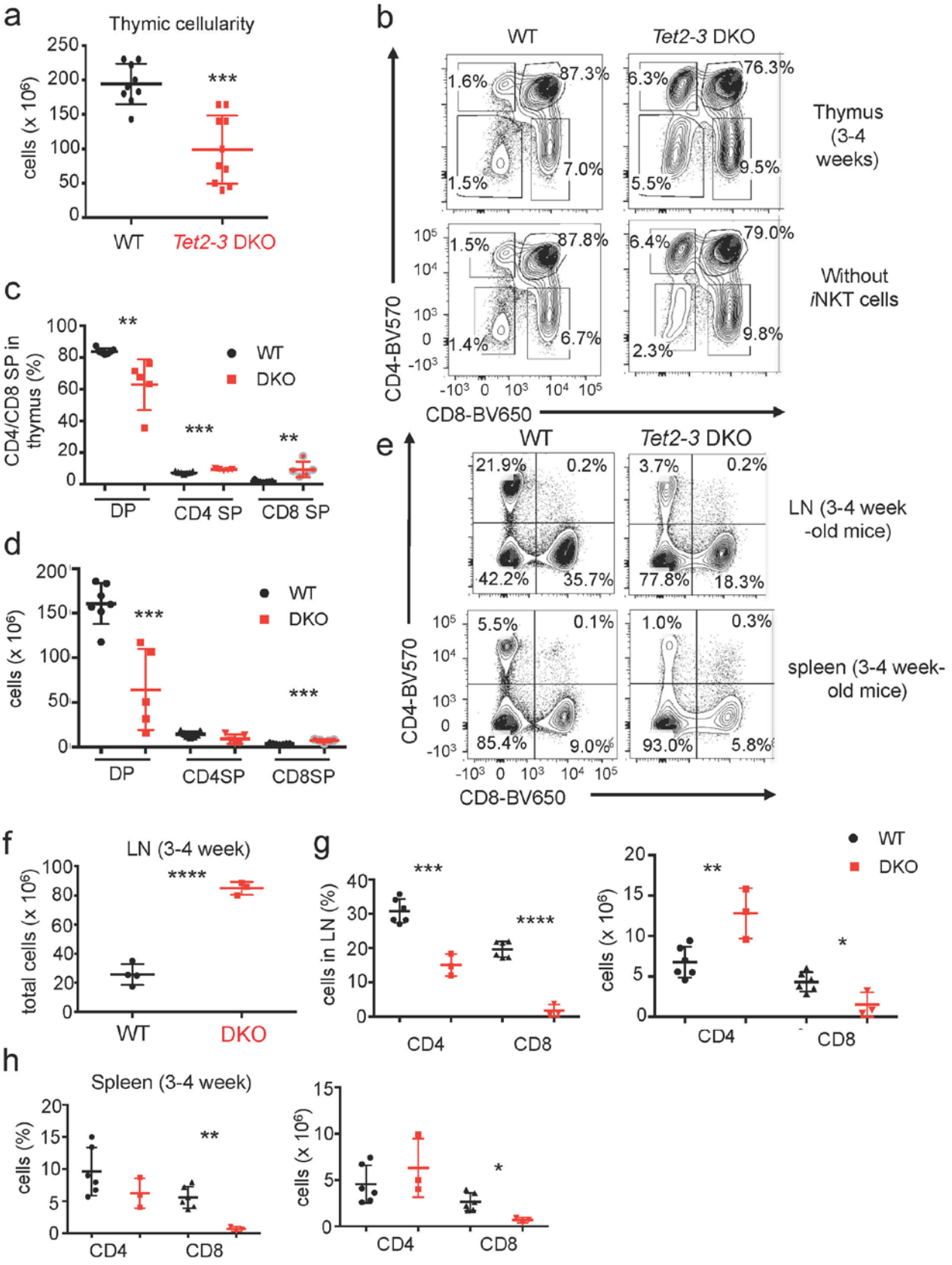
a
Thymic cellularity
cells (x 10⁶)
250
200
150
100
50
0
***
WT
Tet2-3 DKO
b
WT
Tet2-3 DKO
1.6%
87.3%
1.5%
7.0%
6.3%
76.3%
5.5%
9.5%
Thymus (3-4 weeks)
1.5%
87.8%
1.4%
6.7%
6.4%
79.0%
2.3%
9.8%
Without iNKT cells
CD4-BV570
CD8-BV650
c
CD4/CD8 SP in thymus (%)
100
80
60
40
20
0
**
***
**
WT
DKO
DP
CD4 SP
CD8 SP
d
cells (x 10⁶)
200
150
100
50
0
***
***
WT
DKO
DP
CD4SP
CD8SP
e
WT
Tet2-3 DKO
21.9%
0.2%
42.2%
35.7%
3.7%
0.2%
77.8%
18.3%
LN (3-4 week -old mice)
5.5%
0.1%
85.4%
9.0%
1.0%
0.3%
93.0%
5.8%
spleen (3-4 week-old mice)
CD4-BV570
CD8-BV650
f
LN (3-4 week)
total cells (x 10⁶)
100
80
60
40
20
0
****
WT
DKO
g
cells in LN (%)
40
30
20
10
0
***
****
CD4
CD8
cells (x 10⁶)
20
15
10
5
0
**
*
WT
DKO
CD4
CD8
h
Spleen (3-4 week)
cells (%)
20
15
10
5
0
**
CD4
CD8
cells (x 10⁶)
15
10
5
0
*
CD4
CD8

Supplementary Figure 2

Analysis of CD4 and CD8 T cell development in wild type and *Tet2-3* DKO mice.

(a) Thymic cellularity in wild type (n=9) and *Tet2-3* DKO (n=10) mice at 3-4 weeks of age.

(b) *Top,* Analysis of DN, DP, CD4 and CD8 SP thymic subsets defined by surface staining for CD4 and CD8 markers. *Bottom*, Representation of these subsets after gating out *i*NKT cells as defined by $\tilde{\alpha}$GalCer-CD1d and TCRβ staining.

(c) Percentage and **(d),** Number of DP, CD4 SP and CD8 SP cells in the thymus of WT (n=6) and *Tet2-3* DKO (n=5) mice at 3-4 weeks.

(e) Representation of CD4 and CD8 T cells in lymph nodes (LN, *top*) and spleen (*bottom*) of WT and *Tet2-3* DKO mice at 3-4 weeks.

(f) Total number of cells in lymph nodes (LN) of 3-4 week old WT (n=3) and *Tet2-3* DKO (n=3) mice.

(g) Percentage and number of CD4 and CD8 cells in the LN of WT (n=6) and *Tet2-3* DKO (n=3) mice analyzed at 3-4 weeks old.

(h) Percentage and number of CD4 and CD8 cells in the spleen of WT (n=6) and *Tet2-3* DKO (n=3) mice analyzed at 3-4 weeks old.

Data are mean $\pm$ SEM. *P<0.05, **P< 0.01, ***P< 0.001, ****P< 0.0001 (unpaired t test).

At least 3 independent experiments were performed.

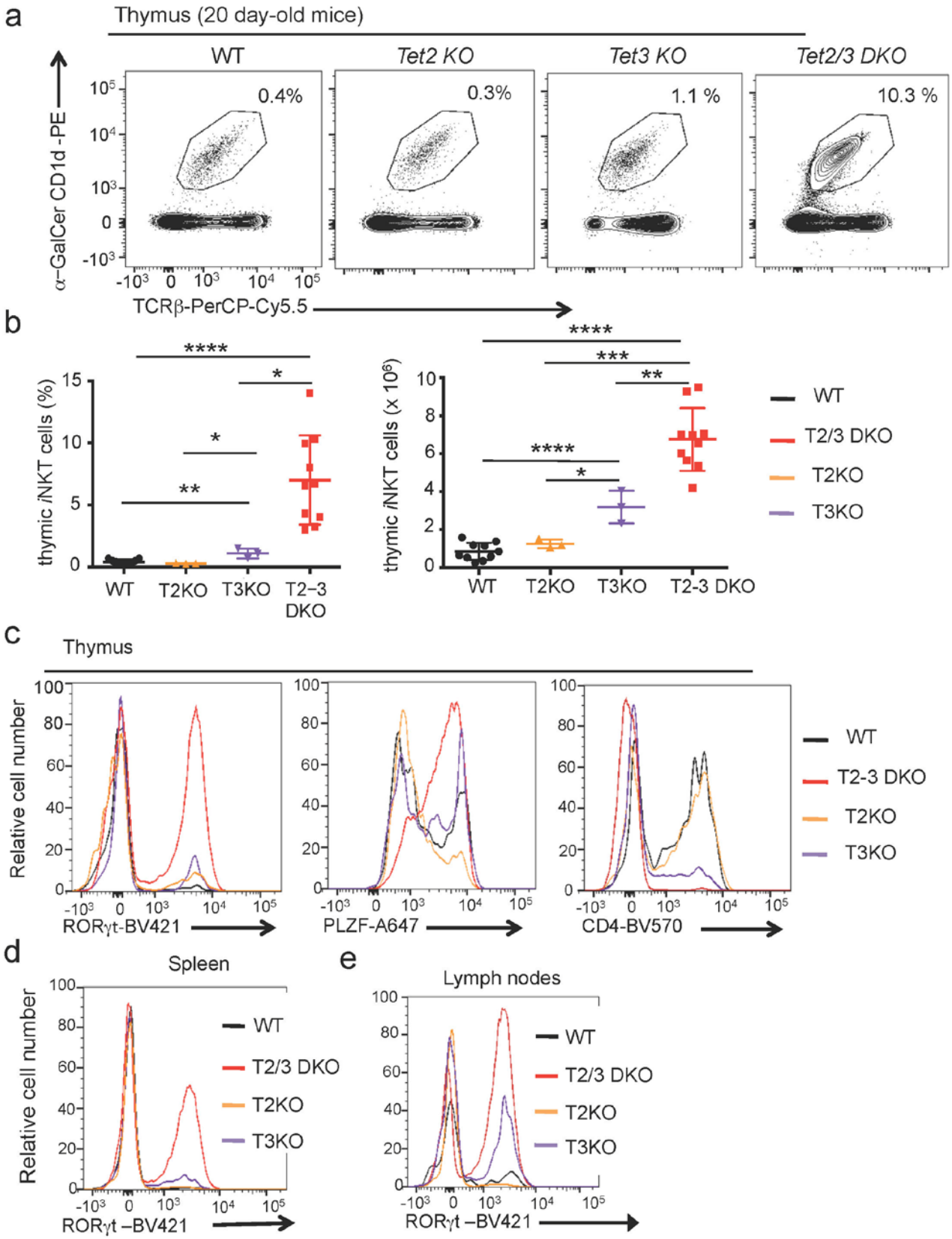

Nature Immunology: doi:10.1038/ni.3630

Supplementary Figure 3

Profound loss of TET proteins is required for dysregulated expansion and function of *i*NKT cells.

(a) *i*NKT cells in the thymus of representative 20 day-old WT versus *Tet2*$^{-/-}$, *Tet3* KO and *Tet2-3* DKO mice, defined by staining with $\tilde{\alpha}$GalCer-CD1d tetramer and anti-TCRβ.

(b) Increased percentages (*left*) and numbers (*right*) of *i*NKT cells in spleens isolated from 4 week-old WT (n=6), T2$^{-/-}$ (T2 KO, n=3), T3 KO (n=3) and *Tet2-3* DKO (n=10) mice.

(c) Histogram evaluating the expression of RORγt *(left)*; PLZF (*center*); and CD4 *(right)* in WT, single *Tet2*$^{-/-}$ (*Tet2* KO), *Tet3* KO, *Tet2-3* DKO thymic *i*NKT cells.

(d, e) Histogram evaluating the expression of RORγt in the spleen **(d)** and lymph nodes **(e)** of WT, single *Tet2*$^{-/-}$, *Tet3* KO, *Tet2-3* DKO *i*NKT cells.

Data are mean $\pm$ SEM. *P<0.05, **P< 0.01, ***P< 0.001, ****P< 0.0001 (unpaired t test)

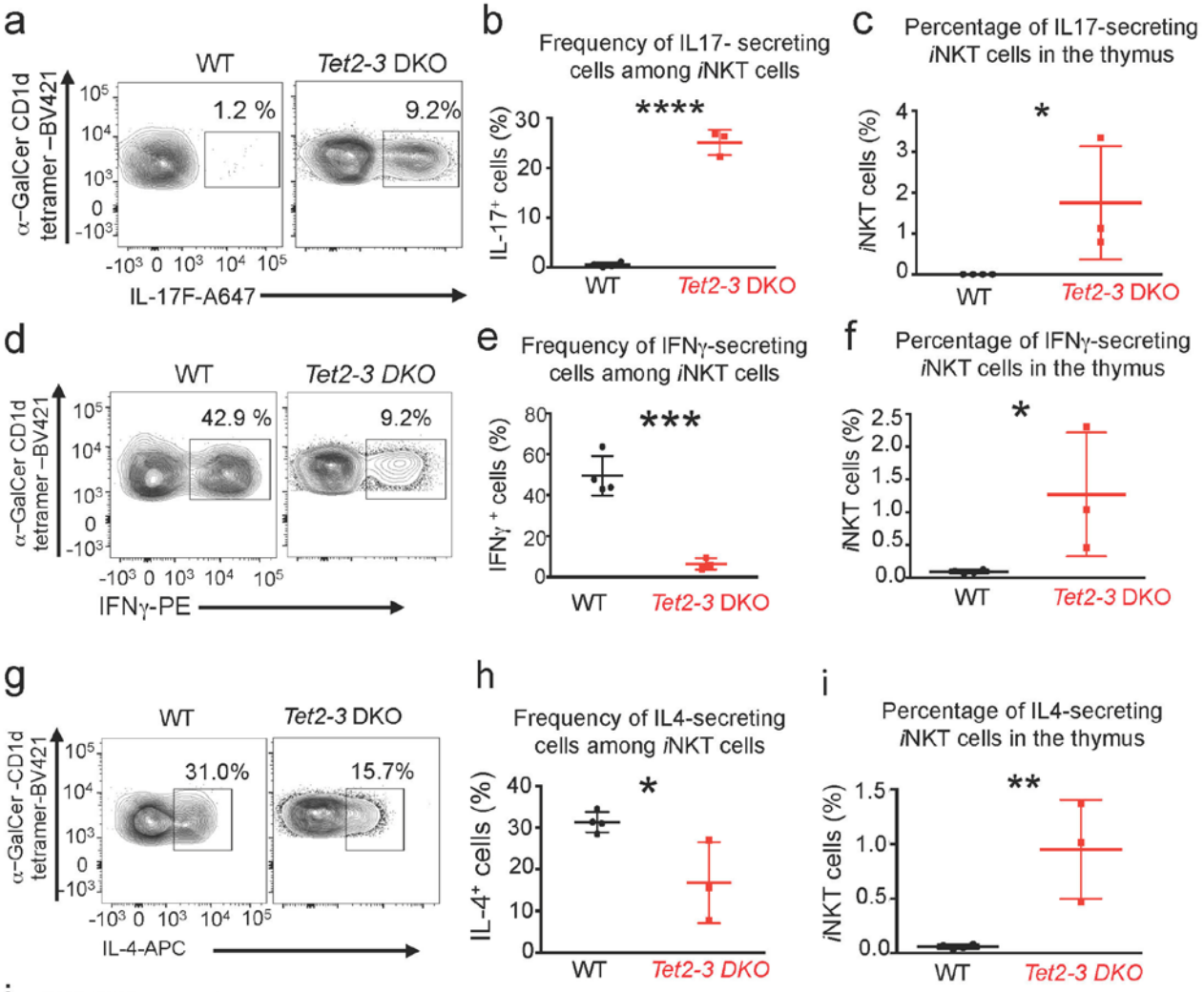
a
WT
Tet2-3 DKO
α-GalCer CD1d tetramer –BV421
1.2 %
9.2%
IL-17F-A647
b
Frequency of IL17- secreting cells among iNKT cells
****
IL-17+ cells (%)
WT
Tet2-3 DKO
c
Percentage of IL17-secreting iNKT cells in the thymus
*
iNKT cells (%)
WT
Tet2-3 DKO
d
WT
Tet2-3 DKO
α-GalCer CD1d tetramer –BV421
42.9 %
9.2%
IFNγ-PE
e
Frequency of IFNγ-secreting cells among iNKT cells
***
IFNγ+ cells (%)
WT
Tet2-3 DKO
f
Percentage of IFNγ-secreting iNKT cells in the thymus
*
iNKT cells (%)
WT
Tet2-3 DKO
g
WT
Tet2-3 DKO
α-GalCer -CD1d tetramer-BV421
31.0%
15.7%
IL-4-APC
h
Frequency of IL4-secreting cells among iNKT cells
*
IL-4+ cells (%)
WT
Tet2-3 DKO
i
Percentage of IL4-secreting iNKT cells in the thymus
**
iNKT cells (%)
WT
Tet2-3 DKO
j
CD8 SP thymocytes
Relative cell number
CD122-PE
CD44-A700
CXCR3-BV421
EOMES-A647
WT
Tet2-3 DKO
k
CD122
****
cells (%)
WT
DKO
CD44
****
WT
DKO
CXCR3
****
WT
DKO
Eomes
****
WT
DKO

Supplementary Figure 4

Cytokine production in *Tet2-3* DKO *i*NKT cells.

(a) Representative flow cytometric analysis of IL17 secretion by $\tilde{\alpha}$GalCer-CD1d tetramer$^+$ TCRβ^+ cells.

(b) Percentage of IL17-secreting *i*NKT cells among total *i*NKT cells.

(c) Percentage of IL17-secreting *i*NKT cells among total thymocytes.

(d) Representative flow cytometric analysis of IFNγ secretion by $\tilde{\alpha}$GalCer-CD1d tetramer$^+$ TCRβ^+ TCR cells.

(e) Percentage of IFNγ-secreting *i*NKT cells among total *i*NKT cells.

(f) Percentage of IFNγ-secreting *i*NKT cells among total thymocytes.

(g) Representative flow cytometric analysis of IL4 secretion by $\tilde{\alpha}$GalCer-CD1d tetramer$^+$ TCRβ^+ cells.

(h) Percentage of IL4-secreting *i*NKT cells among *i*NKT cells.

(i) Percentage of IL4-secreting *i*NKT cells among total thymocytes.

In all cases (a-i) 3 mice per genotype were evaluated in 2 independent experiments.

(j) CD8 SP thymocytes were assessed by flow cytometry for the expression of markers that characterize memory-like CD8 cells: surface markers CD122, CD44, CXCR3 and the transcription factor Eomes.

(k) Percentage of CD8 SP thymocytes that express CD122, CD44, CXCR3 and Eomes. WT (n=3) and *Tet2-3* DKO (n=3) mice. For (j) and (k) 3 independent experiments were performed.

Data are mean $\pm$ SEM. *P<0.05, **P< 0.01, ***P< 0.001, ****P< 0.0001 (unpaired t test)

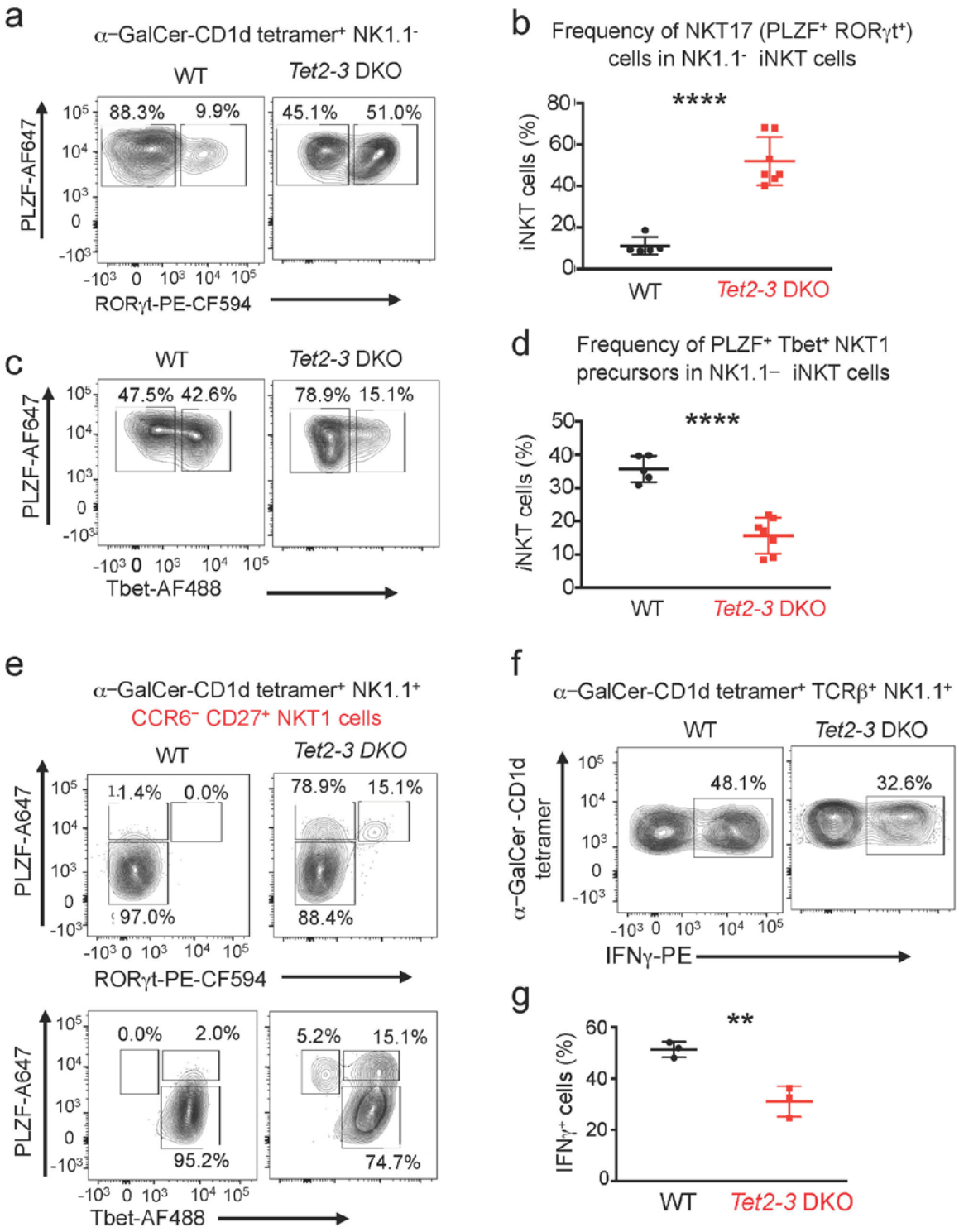

Nature Immunology: doi:10.1038/ni.3630

Supplementary Figure 5

Increase of NKT17 subset and reduction of NKT1 precursors in the NK1.1- *Tet2-3* DKO *i*NKT cells.

(a) Representative flow cytometric analysis of transcription factors PLZF and RORγt in $\tilde{\alpha}$GalCer-CD1d tetramer$^+$ CD24$^-$TCRβ$^+$ NK1.1$^-$ *i*NKT cells reveals dramatic increase of NKT17 subset.

(b) Percentage of *i*NKT cells expressing PLZF and Rorγt (NKT17 subset) among the NK1.1$^-$ *i*NKT cells. n=5 WT mice and 7 *Tet2-3* DKO mice. Data are compiled from 4 independent experiments.

(c) Representative flow cytometric analysis of PLZF and T-bet expression in NK1.1$^-$ *i*NKT cells. The frequency of PLZF$^+$Tbet$^+$ NKT1 precursor cells is reduced. One representative experiment of 4 is shown.

(d) Percentage of *i*NKT cells expressing PLZF and T-bet (NKT1 precursor cells) among NK1.1$^-$ *i*NKT cells. p<0.0001. n=5 WT mice and 7 *Tet2-3* DKO mice. Data are compiled from 4 independent experiments.

(e) Representative flow cytometric analysis of transcription factors PLZF and T-bet in $\tilde{\alpha}$GalCer-CD1d tetramer$^+$ CD24$^-$ TCRβ$^+$ NK1.1$^+$ *i*NKT cells shows expression of RORγt and emergence of an aberrant PLZF^{high} Tbet$^+$ population.

(f) $\tilde{\alpha}$GalCer-CD1d tetramer$^+$ TCRβ$^+$ NK1.1$^+$ WT and *Tet2-3* DKO *i*NKT cells were stimulated ex vivo with PMA and ionomycin. Representative flow cytometric analysis of $\tilde{\alpha}$GalCer-CD1d tetramer$^+$ cells that secrete IFNγ is shown.

(**g**) Percentage of WT and *Tet2-3* DKO $\tilde{\alpha}$GalCer-CD1d tetramer$^+$ CD24$^-$TCRβ$^+$NK1.1$^+$ *i*NKT cells that secrete IFNγ. One of 2 independent experiments is shown. Cells isolated from 3 different mice/ genotype were evaluated.

Data are mean ± SEM. **P< 0.01, ****P< 0.0001 (unpaired t test)

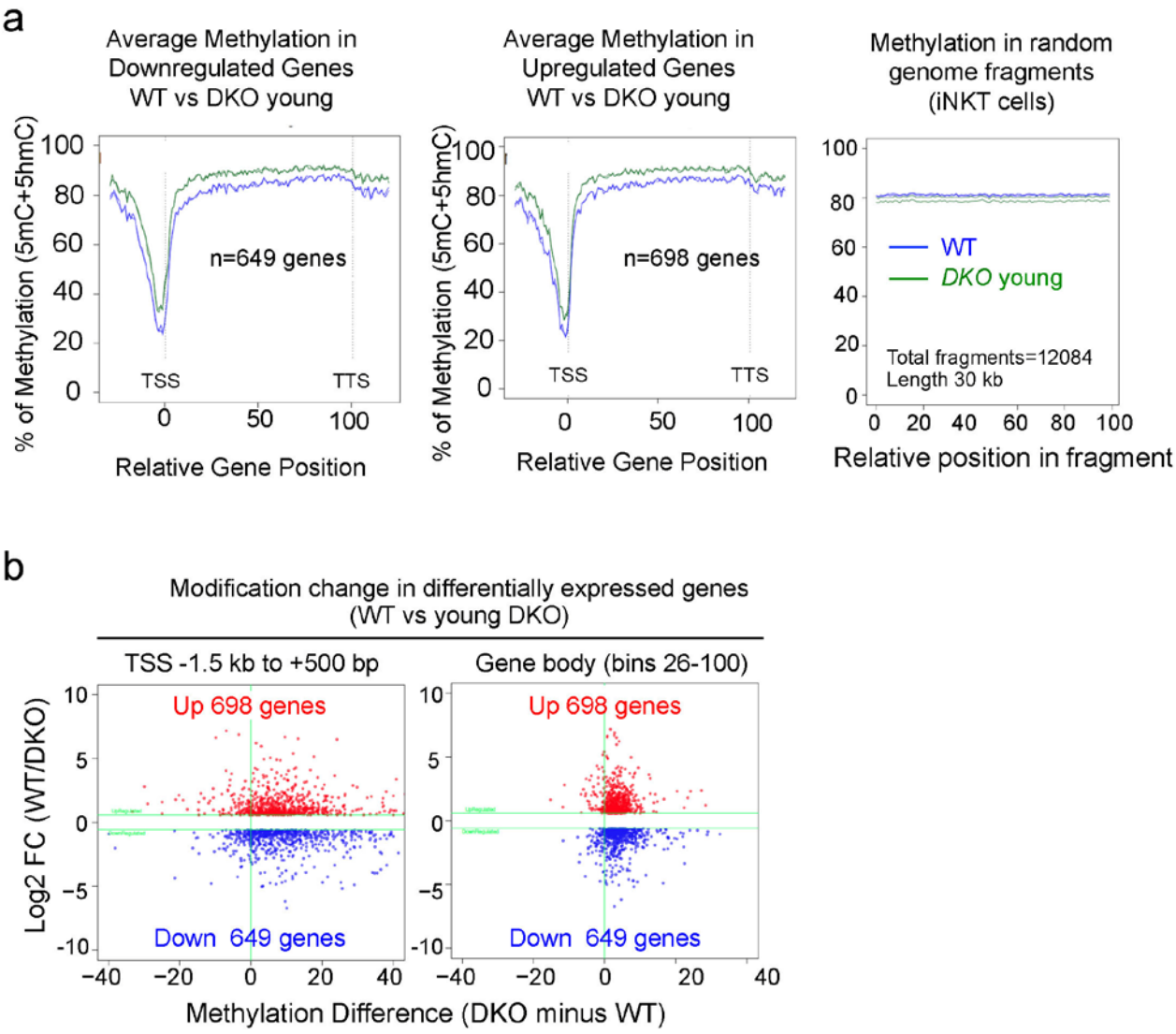
a
Average Methylation in Downregulated Genes WT vs DKO young
% of Methylation (5mC+5hmC)
n=649 genes
TSS
TTS
Relative Gene Position
Average Methylation in Upregulated Genes WT vs DKO young
n=698 genes
Methylation in random genome fragments (iNKT cells)
WT
DKO young
Total fragments=12084
Length 30 kb
Relative position in fragment
b
Modification change in differentially expressed genes (WT vs young DKO)
TSS -1.5 kb to +500 bp
Gene body (bins 26-100)
Up 698 genes
Down 649 genes
Log2 FC (WT/DKO)
Methylation Difference (DKO minus WT)

Supplementary Figure 6

Correlation of DNA modifications (5mC and 5hmC) with gene expression

(a) Composite analysis of methylation (5mC+5hmC) in genes with decreased (*left*, downregulated) or increased (*middle,* upregulated) expression in young *Tet2-3* DKO *i*NKT cells compared to WT. *Right*, Methylation in random genomic fragments.

(b) Methylation changes in the promoter (*left*) and the gene body (*right*) of individual differentially-expressed genes, plotted against the ratio of their expression in WT versus young *Tet2-3* DKO *i*NKT cells. Each dot represents a gene. *Up* (red dots) 698 genes with higher expression in WT compared to *Tet2-3* DKO *i*NKT cells; *Down* (blue dots), 649 genes with lower expression in WT compared to *Tet2-3* DKO *i*NKT cells.

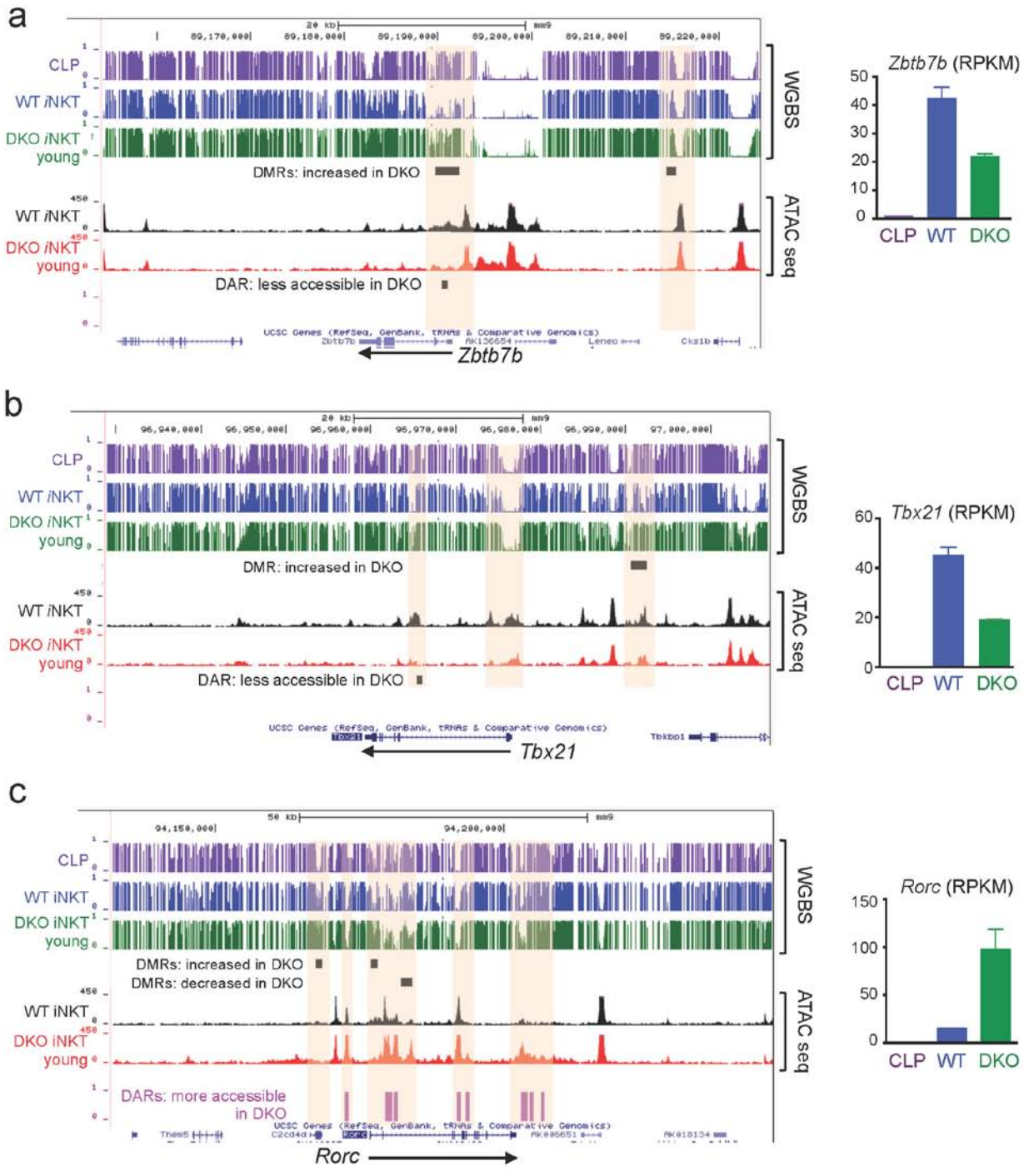
a
CLP
WT iNKT
DKO iNKT young
WGBS
DMRs: increased in DKO
WT iNKT
DKO iNKT young
ATAC seq
DAR: less accessible in DKO
UCSC Genes (RefSeq, GenBank, tRNAs & Comparative Genomics)
Zbtb7b
Zbtb7b (RPKM)
50
40
30
20
10
0
CLP WT DKO
b
CLP
WT iNKT
DKO iNKT young
WGBS
DMR: increased in DKO
WT iNKT
DKO iNKT young
ATAC seq
DAR: less accessible in DKO
UCSC Genes (RefSeq, GenBank, tRNAs & Comparative Genomics)
Tbx21
Tbx21 (RPKM)
60
40
20
0
CLP WT DKO
c
CLP
WT iNKT
DKO iNKT young
WGBS
DMRs: increased in DKO
DMRs: decreased in DKO
WT iNKT
DKO iNKT young
ATAC seq
DARs: more accessible in DKO
UCSC Genes (RefSeq, GenBank, tRNAs & Comparative Genomics)
Rorc
Rorc (RPKM)
150
100
50
0
CLP WT DKO

Supplementary Figure 7

Differentially modified regions (DMRs) and differentially accessible regions (DARs) in genes related to the iNKT cell specification program.

Genome browser views of DNA modification (5mC+5hmC) identified by WGBS and chromatin accessibility identified by ATAC-seq in (**a)** *Tbx21;* **(b)***, Zbtb7b and* **(c)** *Rorc* genes in common lymphoid progenitors (CLP, *purple*), WT *i*NKT cells *(blue*) and young *Tet2/3* DKO *i*NKT cells (*green*). The arrow indicates the direction of transcription. Statistically significant DMRs (*black*) or DARs (*purple for gain of accessibility in Tet2/3* DKO *or black for more accessibility in* WT *iNKT cells*) are indicated by horizontal bars. Selected regions in which modification or/and accessibility is altered from CLP to *i*NKT cells, and then progressively is affected in young *i*NKT cells are highlighted (*salmon shading*). For each gene, the gene expression level (RPKM) in each cell type is indicated.

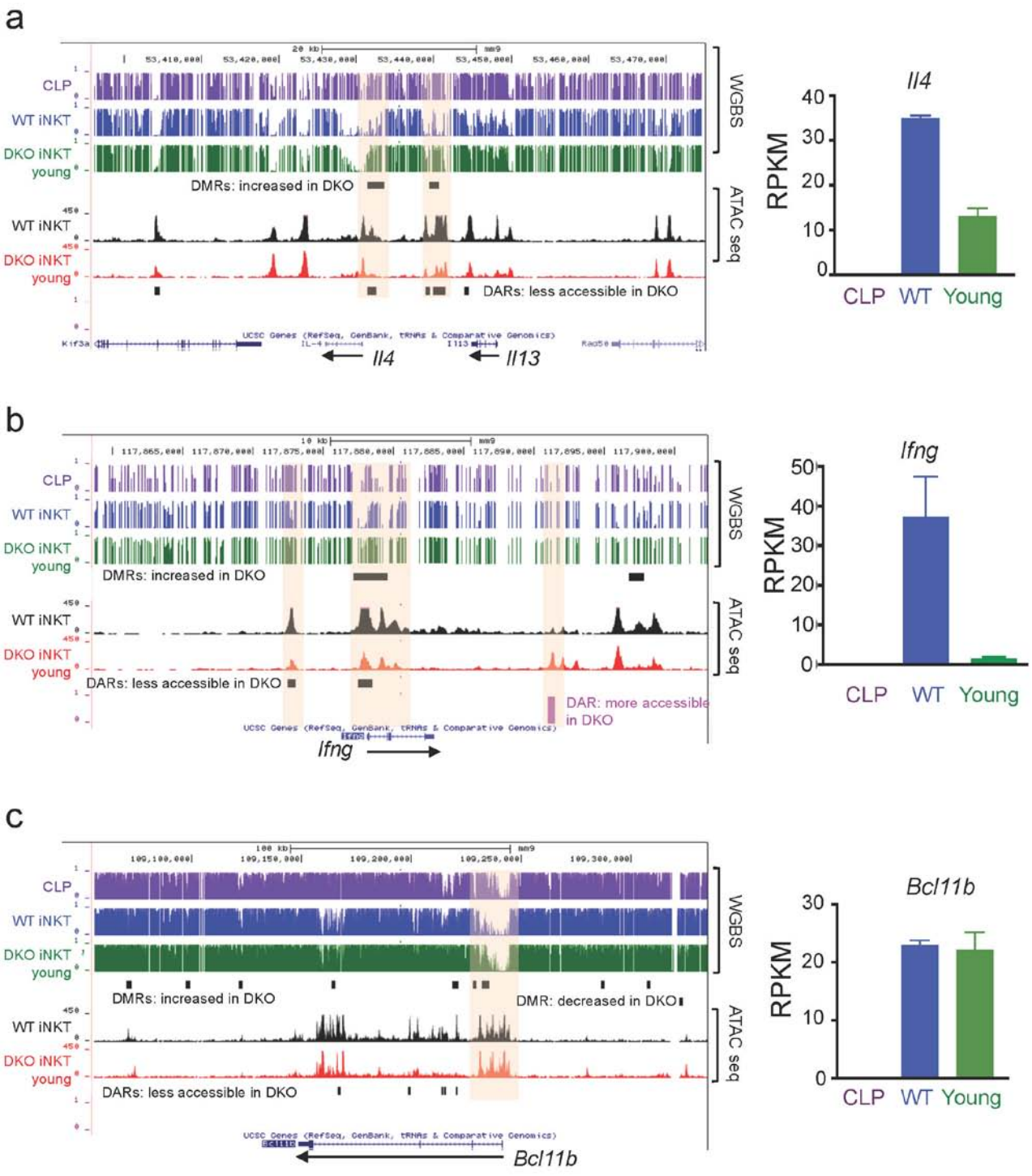
a
CLP
WT iNKT
DKO iNKT young
WGBS
DMRs: increased in DKO
ATAC seq
WT iNKT
DKO iNKT young
DARs: less accessible in DKO
UCSC Genes (RefSeq, GenBank, tRNAs & Comparative Genomics)
Il4
Il13
Il4
RPKM
CLP WT Young
b
CLP
WT iNKT
DKO iNKT young
WGBS
DMRs: increased in DKO
ATAC seq
WT iNKT
DKO iNKT young
DARs: less accessible in DKO
DAR: more accessible in DKO
UCSC Genes (RefSeq, GenBank, tRNAs & Comparative Genomics)
Ifng
Ifng
RPKM
CLP WT Young
c
CLP
WT iNKT
DKO iNKT young
WGBS
DMRs: increased in DKO
DMR: decreased in DKO
ATAC seq
WT iNKT
DKO iNKT young
DARs: less accessible in DKO
UCSC Genes (RefSeq, GenBank, tRNAs & Comparative Genomics)
Bcl11b
Bcl11b
RPKM
CLP WT Young

Supplementary Figure 8

Portraits of DNA modification and gene expression of selected downregulated cytokines and transcription factors in *Tet2-3* DKO *i*NKT cells.

(a)-(c), Genome browser views of DNA modification (5mC+5hmC, identified by WGBS) and chromatin accessibility (identified by ATAC-seq) in **a,** *Il4;* **b***, Ifng and* **c,** *Bcl11b* genes in common lymphoid progenitors (CLP, *purple*), WT iNKT cells *(blue*) and young *Tet2-3* DKO *i*NKT cells (*green*). The arrow indicates the direction of transcription. Statistically significant DMRs (*black*) or DARs (*purple for gain of accessibility in DKO or black for more accessibility in* WT) are indicated by horizontal bars. Selected regions in which DNA modification or/and accessibility is altered from CLP to *i*NKT cells, and then progressively affected in young *i*NKT cells, are highlighted (*salmon shading*). For each gene the expression (RPKM) in each cell type is indicated.

Supplementary Methods

DATA ANALYSIS

RNA-seq data analysis. The reads were mapped to the *Mus musculus* genome (mm9) as well as UCSC transcriptome (downloaded on 05/17/2011) using Tophat[1]. Multimapped reads were discarded. The read counts for each gene were quantified using HTSeq-count tool[2] with parameters: -m union -s reverse. Differential expression analysis was performed using edgeR[3] R package. Genes with RPKM less than 1 in at least two replicates in each compared condition were filtered out before differential-expression calling. Dispersion was estimated as tag-wise dispersion. Genes with FDR<0.05 and at least 1.5-fold difference in expression were identified as differentially expressed. SMARTseq samples were analyzed in the same way except NK1.1^{-} and NKT1 samples were mapped with Tophat2. Read counts for all SMART-seq samples were quantified using HTSeq-count tool with parameters: -m union.

Heatmaps (Fig. 3b). RPKM values were transformed into row-wise *z*-scores and then ordered using hierarchical clustering with Euclidean distance and Ward's minimum variance method.

Heatmap of TFs (Fig. 4e). The $\log_2$ fold changes were ordered and truncated between -2 and 2.

Enriched pathways. Enriched KEGG pathways were derived with GeneTrail tool[4] using default parameters and all UCSC mouse genes as a background.

CMS-IP seq. The reads of CMS-IP and input samples were mapped to the mm9 genome and lambda phage DNA using Bismark mapping tool[5] with default parameters. The mapping was done using the Bowtie 2[6] backend in the paired-end mode. Enriched regions (ERGs) relative to input DNA were detected using the “findPeaks” routine in HOMER [7] with parameters: -style histone –size 500.

In **Fig. 5a**, genes were categorized based on their expression and extended 10% of length upstream from transcription start sites (TSS) and downstream from transcriptional termination sites (TTS). Regions were separated into 101 equal-sized bins and average

counts per million reads values for each bin were calculated. Finally, $\log_2$ ratio between CMS-IP and input was calculated for each bin. Plotting was done using ngs.plot [8].

Identifying tissue-specific enhancers. Tissue-specific enhancer lists can be found: http://chromosome.sdsc.edu/mouse/download.html

Mapping of WGBS data. We employed BSMAP (v2.74)[9] to align paired-end reads from bisulfite-treated samples to the mm9 mouse reference genome allowing 4 mismatches. Reads mapping to multiple locations in the reference genome with the same mapping score were removed as well as the 5′ ends bearing a quality lower than 20 (-R -p 12 -n 0 -v 4 -w 2 -r 1 -q 20).

Bisulfite conversion efficiency was estimated based on cytosine methylation in non-CpG context. For all the samples the bisulfite conversion efficiency was higher than 0.996.
Duplicated reads caused by PCR amplification were removed by BSeQC (v1.2.0)[10] applying a Pvalue cutoff Poisson distribution test in removing duplicate reads(1e-5). Consequently, a maximum of three stacked reads at the same genomic location were allowed and kept for further analysis. In addition, BSeQC was employed for removing DNA methylation artifacts introduced by end repair during adaptor ligation. Overlapping segments of two mates of a pair were reduced to only one copy to avoid considering the same region twice during the subsequent DNA methylation quantification.

Methylation calling. To estimate CpG DNA methylation at both DNA strands, we executed the methratio.py script, from BSMAP (v2.74)[9] (-t 0 -g 1 -x CG -i correct).

DMR discovery -BSseq-. To identify differentially methylated cytosines (DMCs), pair-wise comparisons between different groups [CLPs (n=2 technical replicates), wild-type (n=2 biological replicates) and *Tet2-Tet3* DKO (n=2 biological replicates) *i*NKT cells] were performed with BSseq (v1.2.0)[11]. We required each tested CpG to be covered by at least 2 reads in each of the samples. We kept 2% of the most significantly different CpGs for the subsequent determination of DMRs, defined as more than 5 adjacent CpG with more than 10% increase/decrease and no more than 500 bp away from one another. From those pre-determined DMRs we filtered those who had a median change of higher than 10% using a FDR of 5%. DMRs with at least 25% difference in

5mC+5hmC were used to generate the heatmap in **Figure 6a**. CLP data for two technical replicates are from[12] (accession code SRX852183).

Annotation of DMRs. We used annotatepeak.pl script from HOMER[7] suite to annotate the Hyper- and Hypo- methylated DMRs to a region in the genome. DMRs falling inside 2000 bp upstream and 500 bp downstream of TSS were defined as DMR falling in promoter region. All the other functional annotations were retrieved as they are from annotatepeak.pl table results, i.e. exons, introns, 3′ , 5′ and intergenic regions. The same procedure was conducted using all the CpGs in the mm9 genome, used as control for further comparisons.

Identification of DMRs overlapping with 5hmC (CMS-IP). *Tet2-Tet3* DKO DMRs with at least 20% difference when compared to wild-type *i*NKT cells were identified (10,945 and 767, respectively). These were overlapped with CMS-IP peaks (5hmC peaks from wild-type *i*NKT cells) using bedtools intersect and a threshold of 50% minimum region intersection. We obtained 4568 more-methylated regions and 10 less-methylated regions in DKO-intersecting 5hmC peaks. The results are shown in Table 1.

Correlation of DNA modifications (5mC and 5hmC) with differential gene expression. The distance from the transcription start site (TSS) to the transcription termination site (TTS) for each differentially expressed gene was divided into 100 bins. The average change in DNA modification within each gene body (bins 26-100) and each promoter (+/- 2 kb relative to TSS) was calculated. The values against the $\log_2$-fold change in expression of the corresponding gene were plotted. The data of this analysis are shown in **Supplementary Fig. 6b**.

Discovery and Anotation of differentially accessible regions (DARs).

Mapping: For each sample, paired end ATAC-seq data was mapped against the mm9 using *bowtie* [13] (-p 8 -m 1 --best --strata -X 2000 -S --fr --chunkmbs 1024). Unmapped reads were processed with *trim galore* [14] and remapped using bowtie with the same parameter settings as described above. Sequencing reads mapping to the reference genome in this second round were merged with the initial mapping results. The merged results were filtered for duplicated reads using PICARD tools 1.94

(http://picard.sourceforge.net) and reads mapping to the mitochondrial DNA (chrM) were removed using samtools[15].

Identification of Accessible Regions. To identify accessible regions per sample, ATAC-seq mapping results were processed with *MACS2* [16] (callpeak -f BAMPE -g mm --nomodel --shiftsize 75 -q 0.01 --keep-dup 10 --call-summits). Reproducible accessible regions per condition were defined by calculating the Irreproducibility Discovery Rate[17]. Reproducible accessible regions per condition were merged, resulting in 27,913 and 26,563 accessible regions in *Tet2-Tet3* DKO young or wild-type *i*NKT cells, respectively.

Differentially Accessible Regions. To identify genomic regions preferably accessible in wild-type or *Tet2-Tet3 DKO* young *i*NKT cells, mapped paired-end ATAC-seq data was quantified at previously defined accessible regions in *Tet2-Tet3 DKO* young and wild-type *i*NKT cells using MEDIPS 1.21.3. (quantile=T, fold change ≥ $|\log_2(2)|$, FDR ≤ 0.05, minrowSum=10). The resulting 3,162 and 2,711 genomic regions preferably accessible in *Tet2-Tet3* DKO young or wild-type *i*NKT cells, respectively, are visualized in the MA plot in **Fig. 7a**.

Identification of DARs marked by 5hmC in wild-type *i*NKT cells**.** DARs were overlapped with CMS-IP peaks (5hmC enriched regions in wild-type *i*NKT cells) using bedtools intersect requiring a threshold of 50% minimum region intersection resulting in 87 5hmC marked DARs preferably accessible in *Tet2-Tet3* DKO young *i*NKT cells and in 1,018 DARs preferably accessible in wild-type *i*NKT cells.

Transcription factor motif enrichment in DARs. Unique peaks for each condition were used to do a motif search with HOMER's findMotifsGenome.pl.[7]. The commonly accessible regions between wild-type and *Tet2-Tet3* DKO *i*NKT cells were provided as background to the findMotifsGenome.pl model. Besides masking repetitive elements, we used the default parameters of the program.

References related to Supplementary Methods

1. Trapnell C, Pachter L, Salzberg SL. TopHat: discovering splice junctions with RNA-Seq. *Bioinformatics* 2009, **25**(9)**:** 1105-1111.

2. Anders S, Pyl PT, Huber W. HTSeq-a Python framework to work with high-throughput sequencing data. *Bioinformatics* 2015, **31**(2)**:** 166-169.

3. Robinson MD, McCarthy DJ, Smyth GK. edgeR: a Bioconductor package for differential expression analysis of digital gene expression data. *Bioinformatics* 2010, **26**(1)**:** 139-140.

4. Backes C, Keller A, Kuentzer J, Kneissl B, Comtesse N, Elnakady YA*, et al.* GeneTrail--advanced gene set enrichment analysis. *Nucleic acids research* 2007, **35**(Web Server issue)**:** W186-192.

5. Krueger F, Andrews SR. Bismark: a flexible aligner and methylation caller for Bisulfite-Seq applications. *Bioinformatics* 2011, **27**(11)**:** 1571-1572.

6. Langmead B, Trapnell C, Pop M, Salzberg SL. Ultrafast and memory-efficient alignment of short DNA sequences to the human genome. *Genome biology* 2009, **10**(3)**:** R25.

7. Heinz S, Benner C, Spann N, Bertolino E, Lin YC, Laslo P*, et al.* Simple combinations of lineage-determining transcription factors prime cis-regulatory elements required for macrophage and B cell identities. *Molecular cell* 2010, **38**(4)**:** 576-589.

8. Shen L, Shao N, Liu X, Nestler E. ngs.plot: Quick mining and visualization of next-generation sequencing data by integrating genomic databases. *BMC genomics* 2014, **15:** 284.

9. Xi Y, Li W. BSMAP: whole genome bisulfite sequence MAPping program. *BMC bioinformatics* 2009, **10:** 232.

10. Lin X, Sun D, Rodriguez B, Zhao Q, Sun H, Zhang Y*, et al.* BSeQC: quality control of bisulfite sequencing experiments. *Bioinformatics* 2013, **29**(24)**:** 3227-3229.

11. Hansen KD, Langmead B, Irizarry RA. BSmooth: from whole genome bisulfite sequencing reads to differentially methylated regions. *Genome biology* 2012, **13**(10)**:** R83.

12. Kieffer-Kwon KR, Tang Z, Mathe E, Qian J, Sung MH, Li G*, et al.* Interactome maps of mouse gene regulatory domains reveal basic principles of transcriptional regulation. *Cell* 2013, **155**(7)**:** 1507-1520.

13. Langmead B, Salzberg SL. Fast gapped-read alignment with Bowtie 2. *Nature methods* 2012, **9**(4)**:** 357-359.

14. Krueger F. Trim Galore: A wrapper tool around Cutadapt and FastQC to consistently apply quality and adapter trimming to FastQ files, with some extra functionality for MspI-digested RRBS-type (Reduced Representation Bisufite-Seq) libraries. 2015. Available: http://www.bioinformatics.babraham.ac.uk/projects/trim_galore/. 2015.

15. Li H, Handsaker B, Wysoker A, Fennell T, Ruan J, Homer N*, et al.* The Sequence Alignment/Map format and SAMtools. *Bioinformatics* 2009, **25**(16)**:** 2078-2079.

16. Zhang Y, Liu T, Meyer CA, Eeckhoute J, Johnson DS, Bernstein BE*, et al.* Model-based analysis of ChIP-Seq (MACS). *Genome biology* 2008, **9**(9)**:** R137.

17. Li Q, Brown, J. B., Huang, H., & Bickel, P. Measuring reproducibility of high-throughput experiments. . *The annals of applied statistics* 2011**:** 1752-1779.